Scientific Research Publishing

Journal of Computer and Communications, 2026, 14(6), 13-26
https://www.scirp.org/journal/jcc
ISSN Online: 2327-5227
ISSN Print: 2327-5219

Bio-Inspired Physical Reservoir Computing Based on Organic Electrochemical Transistors for Temporal Pattern Recognition

Jingqi Wang*, Dongsheng Zhang

Shanghai High School International Division, Shanghai, China
Email: *cherlynwjq0626@163.com

How to cite this paper: Wang, J.Q. and Zhang, D.S. (2026) Bio-Inspired Physical Reservoir Computing Based on Organic Electrochemical Transistors for Temporal Pattern Recognition. *Journal of Computer and Communications*, **14**, 13-26.
https://doi.org/10.4236/jcc.2026.146002

Received: March 24, 2026
Accepted: June 15, 2026
Published: June 18, 2026

Abstract

The increasing demand for real-time and energy-efficient artificial intelligence (AI) processing exposes fundamental limitations of traditional von Neumann architectures. Neuromorphic computing, inspired by biological neural systems, offers a promising alternative by integrating memory and computation within dynamic physical substrates. Here, we demonstrate organic electrochemical transistors (OECTs) based on PEDOT:PSS as dynamic nodes for physical reservoir computing (PRC). OECTs exhibit coupled ionic-electronic transport, volumetric doping, and intrinsic short-term memory arising from ion diffusion, enabling nonlinear temporal signal transformation without recurrent circuitry. Flexible high-resolution OECT devices were fabricated via multilayer photolithography and characterized electrically. Under pulsed gating, the devices exhibit synaptic behaviors including paired-pulse facilitation, spike-timing-dependent plasticity, and frequency-dependent plasticity. Temporally encoded 4 × 4 MNIST digit images were applied as gate voltage sequences. The resulting drain current waveforms were analyzed to extract dynamic features and classified using a softmax regression model. The system achieved an average recognition accuracy of 78.6% without internal weight training. These results establish OECT-based PRC as a scalable, low-power, and bio-compatible neuromorphic hardware platform for temporal information processing.

Keywords

Organic Electrochemical Transistors (OECT), Physical Reservoir Computing, Neuromorphic Computing, PEDOT:PSS, MNIST Classification, Bio-Electronic

1. Introduction

The rapid increase in need for current AI as well as energy-effective AI already questions the abilities to the normal von Newmann-structure. These older computers separated their physical memory spaces from processor cores, which made it difficult for them to hold all the new neural nets at once, because that takes up lots of time going between memory storage places, and using power all over like this huge "Memory Wall" effect on these newer nets, that require super high throughput of data transfer (lots) [1]. To fight such inefficient ways of doing stuff neuromorhic computing is becoming an alternative. Following the biological brain's approach this will include integration computation and memorization as events driven system in series, which would be capable of making significant leap forward, when working with temporal information regarding to its use of power [2].

Of the many different neuromorphic architectures out there, it is Reservoir Computing (RC) that gets called upon as being pretty strong at doing work with stuff changing over time [3]. In contrast to conventional RNNs, which entail costly and generally troublesome to train all those inner-connections that could easily become stuck during learning (RNN) RC takes this reservoir which is an inherently nonlinear system which maps the incoming signal into some big, messy space via that reservoir and then all you get are very simple linear mappings from there forward out of whatever did with the reservoir. Therefore the rest of the network can be left untrained with reduced computation cost. The early RC implementations were based on software-simulated Echo State Networks while later works concentrated on Physical Reservoir Computing (PRC) in which the nonlinear dynamic of physical substrate substitute software defined neuron [4]. There's all sorts of material that people use: Optical Systems and Memristor Systems. But many of the inorganic ones also run into problems of needing high voltages, being hard to make, and sometimes not being friendly to living things.

Organic electrochemical transistors (OECTs) are the most popular choice as the PRC nodes [5] as well recently. Typically, they use the conjugated-polymer material, PEDOT:PSS and they do it through very specific process where they use coupled ionic and electronic transport along with changes in volume, *i.e.*, volumetric doping. Ion can pass into polymer bulk via this method which makes channel's conductance vary over time and looks like living synapse with short-term memory (STM) and change-ability (plasticity) [6]. In contrast to surface-gated silicon transistors, OECT has much higher transconductance at sub-Volt levels, and it is also naturally solution-processable/flexible.

Though there is some strength for it here but there's no sort of an exhaustive or systematic kind of presentation in this field, showing a transition between what happens at a very small scale, like just looking at things with your magnifying glass up close and the type of complex stuff actually want to do, like having lots of different groups of information being put together all at once. Current studies tend to consider individual synaptic phenomena such as paired pulse facilitation in iso-

lation rather than within the functional computing framework of recognizing patterns. In terms of PRC system, specifically, robust implementations using flexible OECT arrays for digitized images are still in their early days.

In our case here is a work regarding reporting a high performance but also a flexible PR system using PEDOTPSS OECT in recognition of a temporal sequence. Comprehensive approach: scalable microfabrication to algorithms. We built up an array by means of multilayer photolithography, and it has high resolution with obvious synaptic like behavior such as PPF, STDP. System computational power validation with use of the MNIST handwritten digit data set where we encoded spatial pixel info into temporally gated voltage sequences. By utilizing the OECT's ionic-electronic fading memory, the single-node reservoir effectively transformed the input signal space into a much higher dimensional space with a simple Softmax regression readout, obtaining a classification accuracy of 78.6%. This paper points out that maybe OECT can be used as building block for low power and flexible bio inspired system.

2. Methodology

2.1. Data Collection and Dataset Description

In order to examine if the proposed OECT-based physical reservoir computing (PRC) has time computing ability, the MNIST handwritten digit dataset was used. MNIST is an established dataset for studies in both machine-learning and neuromorphic computing and first appeared in work of LeCun *et al.* It contains 70,000 grayscale pictures of handwritten figures (0 - 9): 60,000 training and 10,000 testing. Image size 28 × 28 with pixel intensity 0 - 255.

In this work uses a down sampled version by a factor of 4x4 obtained via spatial down sampling on the 28 × 28 images. The purposeful low dimension is done so because there's just that few amount of virtual nodes inside of the single-OECT times multiplexer's reservoir system, thus ensuring both hardware dynamic and input size are compatible with each other (Figure 1). Representative Examples of Original MNIST Dataset.

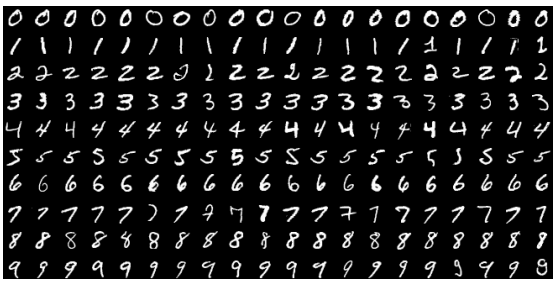

Figure 1. Representative samples from the MNIST handwritten digit dataset.

To establish a consistent experimental protocol, a subset of 1,116 images was selected from the MNIST dataset without data augmentation. This subset was split using a strictly class-balanced scheme: 16 images were used for classifier training,

500 independent samples were used for hyperparameter validation, and the remaining 600 samples were reserved for final testing. All preprocessing was performed digitally prior to waveform encoding.

2.2. Microscopic Physics and Device Modeling of OECTs

The OECTs operation is based on the combined movement of both ions and electron's inside of Organic Mixture of Ionic & Electron Conductor (OMIEC) [7]. In Figure 2 we can see that the device uses PEDOT:PSS as its active channel material; the conducting $PEDOT^+$ chains are counterbalanced by the insulating PSS^- chains. A positive gate voltage (V_G) is applied. Cation like H^+, Na^+ from electrolyte will be pushed into the polymer bulk. These cations take up for the negative charge on PSS^- chains, thus making it possible to have less dopant concentration in PEDOT and consequently lower hole concentration.

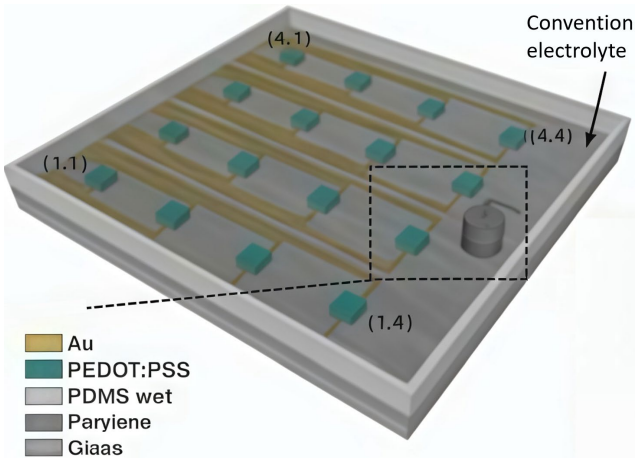

Figure 2. Formation of OECT.

This volumetric doping mechanism allows for a much higher transconductance compared to surface-gated transistors [8]. Based on the Bernards-Malliaras model, the steady-state drain current (I_D) is governed by the following relationship:

$$I_D = \frac{G_0 L}{d}\left(1 - \frac{V_G - V_{off}}{V_P}\right)V_D \tag{1}$$

where G_0 is the peak transconductance, V_P is the pinch-off voltage, and V_{off} is the offset voltage. Beyond steady-state, the device behavior is dictated by the ionic diffusion time constant $\tau = R_s C_{vol}$. As the ions drift and diffuse through the polymer matrix, they create a transient current response that does not immediately decay when the input ceases. This provides the "fading memory" effect—a critical prerequisite for reservoir computing, enabling the device to encode temporal information into its instantaneous state.

2.3. Theoretical Framework of Reservoir Computing (RC)

Reservoir Computing is a specialized recurrent neural network (RNN) architec-

ture designed to minimize training complexity while maximizing temporal processing capabilities. As illustrated in Figure 3 and Figure 4, a standard RC system comprises three distinct layers:

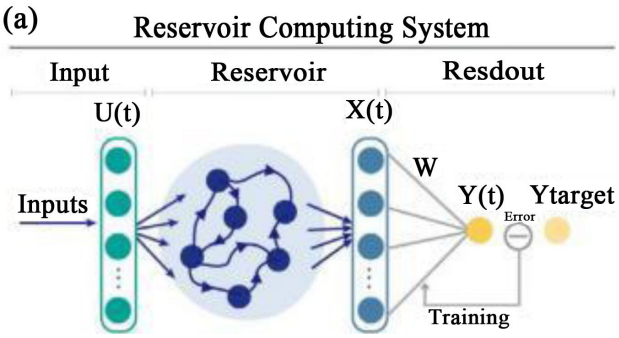

Figure 3. Basic structure of reservoir computing.

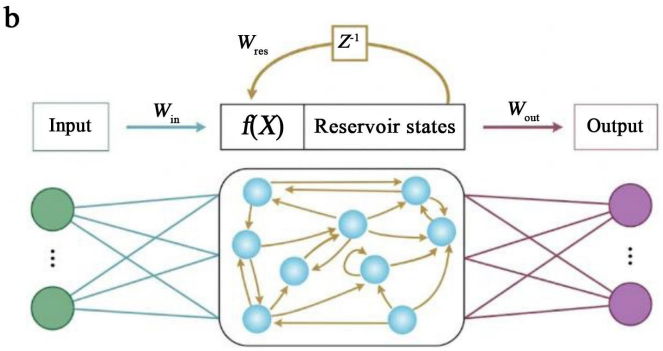

Figure 4. Implementation of physical reservoir using an OECT device.

1) Input Layer: Maps the external signal into the reservoir space via a fixed weight matrix W_{in}.

2) Reservoir: A high-dimensional dynamical system that transforms inputs into complex nonlinear states. In traditional frameworks like the Echo State Network (ESN) and the Liquid State Machine (LSM), this is typically a large, sparse network of nonlinear oscillators or neurons.

3) Readout Layer: A simple linear layer that extracts the final result from the reservoir states through a trainable matrix W_{out}.

The RC most notable strength comes out from it having "Echo State Property," making sure reservoir state stays as a one-to-one link of former inputs' past story [9]. In this paper, we utilize a single physical OECT combined with Time-Division Multiplexing (TDM) to construct the physical reservoir, offering a simplified alternative to complex recurrent neural networks [10]. Here, we explicitly define a "device" as a single physical OECT fabricated on the substrate, and a "channel" as the electrical pathway within that specific device. To process temporal data using a single device, we introduce "virtual nodes," which are defined as discrete time-sampling points extracted along the continuous transient current response of the device under TDM. Although an array of 16 devices was fabricated to ensure sta-

tistical reliability and uniform transfer characteristics, the temporal sequence recognition task reported herein relies entirely on the dynamic virtual nodes generated by a single device. The exact signals entering the classifier are the dynamic feature vectors extracted from these virtual node current responses.

2.4. Mathematical State Transition and Data Encoding

The mathematical representation of the reservoir state $x(n)$ at discrete time n is defined by:

$$x(n) = f\left(W_{in} \cdot u(n) + W_{res} \cdot x(n-1) + b\right) \tag{2}$$

This formulation follows the standard RC state-update framework. where $f(\cdot)$ represents the nonlinear activation function, which is naturally provided by the OECT's nonlinear transconductance and ionic dynamics. The input $u(n)$ consists of temporally encoded data (e.g., MNIST pixel intensities converted into voltage pulse widths or amplitudes).

For the 4 × 4 MNIST recognition task, the spatial pixels are flattened into a temporal sequence. As these pulses pass through the OECT, the device's intrinsic short-term memory (STM) and plasticity-governed by ion-electronic coupling-enable temporal information integration, consistent with previously reported hardware reservoir implementations based on dynamic devices [11]. The final output $y(n)$ is generated by:

$$y(n) = \text{Softmax}\left(W_{out} \cdot X + B_{out}\right) \tag{3}$$

where X is the collected feature vector from the OECT's transient responses. This approach enables the system to capture spatiotemporal correlations of handwritten digits while maintaining significantly lower training complexity than conventional deep learning architectures.

2.5. Delay-Memory Task and Memory Capacity

To quantify the intrinsic short-term memory of the OECT reservoir, a delay-memory task was employed. The memory capacity (MC) was calculated as $MC = \sum_{k=1}^{k_{\max}} r_k^2$, where r_k is the Pearson correlation coefficient between the reconstructed output and the input delayed by k time steps. The memory window of 7 - 9 pulses reported here represents an average value obtained over 10 repeated experimental trials.

3. Experiment Design

3.1. Fabrication of PEDOT:PSS-Based OECT Devices

An experiment is done with some bendy Organic electro-chemical transistor (OECT) which is used as a physical reservoir node in the computation. Device fabrication process of OECT is shown in **Figure 5**. Fabrication was accomplished by a fine-resolution, flexible version of the photolithographic technique. All of the devices were fabricated on rigid glass slides for easy patterning purposes, although

the resulting structure is designed to remain detached for ease of use creating a freestanding flexible device.

It started off with getting those pieces clean from all of its dust, we just used plain old ethyl alcohol plus some fancy oxygen plasma to make sure nothing bad was sticking around on top of it so that our little piece could stick really well to whatever material came next in line. And then after spin coating, they're doing some curing at high temps like 120˚C - 250˚C to get this cross linked Polyimide Film (PI). It provided mechanics for what is after.

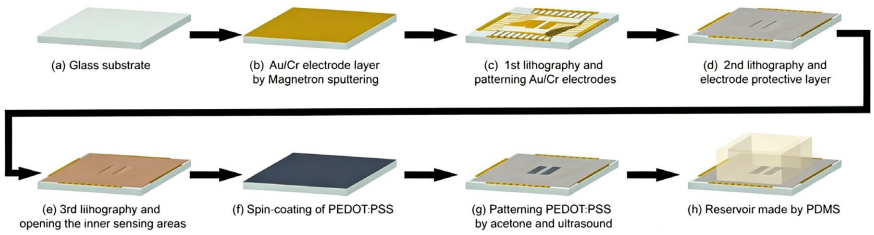

Figure 5. Steps of constructing an OECT.

Next, Cr/Au (5 nm/50 nm) electrodes were deposited via electron beam evaporation after photolithographic patterning and lift-off, defining the source and drain contacts. A second layer of PI was applied as an insulating dielectric and selectively etched via reactive ion etching (RIE) to create contact windows and channel areas. A thick photoresist served as the etching mask to ensure channel exposure while preserving the rest of the structure.

The PEDOT:PSS channel was deposited by spin coating from an aqueous dispersion with added DMSO and GOPS to enhance conductivity and crosslinking. The multilayer PEDOT:PSS structure after patterning is shown in **Figure 6**. The film was annealed at 120˚C to remove residual solvents. A germanium (Ge) sacrificial layer was then deposited (100 nm) and patterned on top of the PEDOT:PSS using standard photolithography. This Ge layer acted as a hard mask for subsequent dry etching of the PEDOT:PSS channel.

ICP-RIE was used to etch both the Ge and PEDOT:PSS layers sequentially, yielding a finely patterned active region. The Ge layer was subsequently dissolved in deionized water due to the solubility of GeO_2, revealing the final device geometry. The entire PI-based device could then be gently peeled from the glass substrate due to weak adhesion, resulting in a fully flexible, fully patterned OECT.

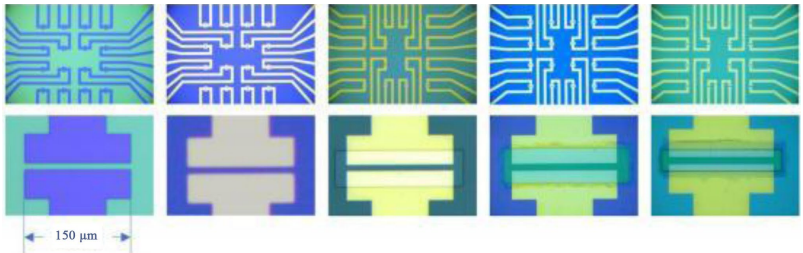

Figure 6. PEDOT:PSS layers.

3.2. Morphological and Structural Characterization

We use optical and scanning electronic microscopy (SEM) to evaluate its form. Optical/Microscopic representative image for patterned PEDOT:PSS channel is displayed in Figure 7. It had the uniform electrode patterning confirmed as well as precise channel definition that had a small amount of residual material/ delamination. The PEDOT:PSS domain was observed having phase-separated microstructural characteristics, having the PEDOT-rich areas inside of a PSS structure. And it would have an effect on the ion accessibility as well as the charge transportation and was then correlated to the electrical and synaptic activity.

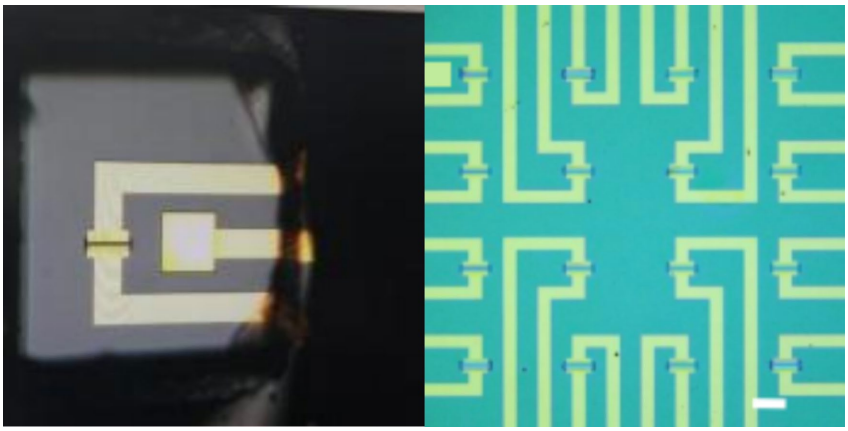

Figure 7. PEDOT:PSS patterning.

3.3. Electrical Measurement Setup

All electrical measurements were performed using a three-terminal setup. The applied square pulse waveform and corresponding transient current response are shown in Figure 8. AnAg/AgCl reference electrode served as the gate and was inserted into a drop of 0.1 M NaCl aqueous electrolyte placed over the channel region. Source-drain current $\left(I_{DS}\right)$ was recorded using a semiconductor parameter analyzer, while gate voltage $\left(V_G\right)$ was applied as either aDC bias or pulse waveform.

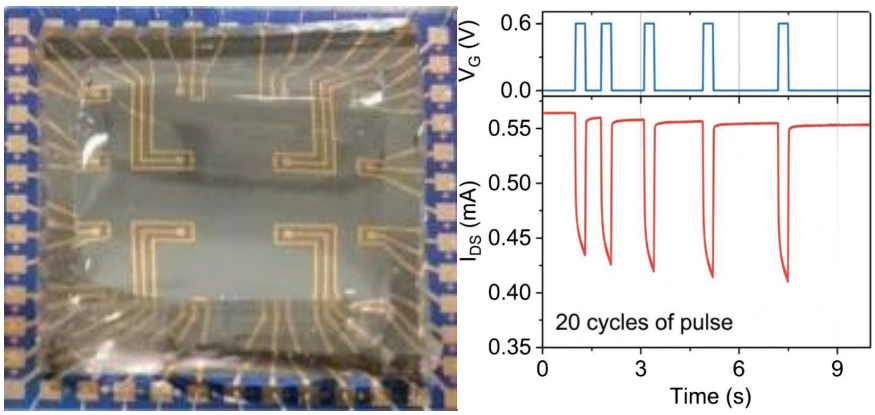

Figure 8. Square pulse input and corresponding current response.

Transfer curves $\left(I_{DS}/V_G\right)$ were obtained at fixed V_{DS} (typically −0.6 V) by sweeping V_G from +0.9V to -0.1V and back. The transfer characteristics of 16 representative devices are summarized in Figure 9. Transconductance $\left(gm = \partial I_{DS}/\partial V_G\right)$ was extracted from the linear regime. All measurements were repeated for at least five cycles to assess stability and repeatability.

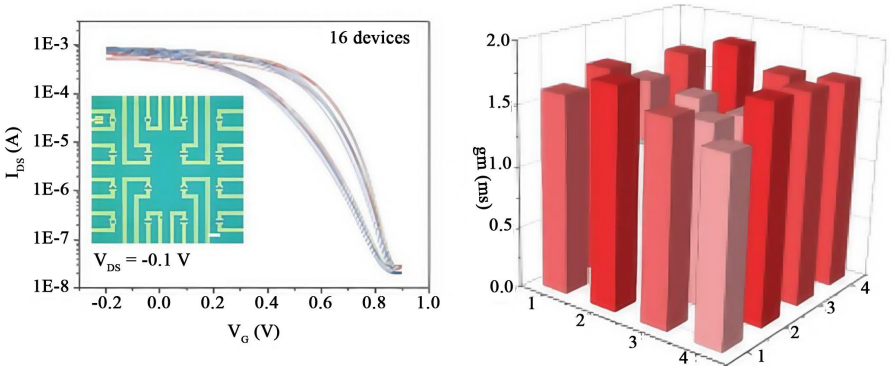

Figure 9. Transfer curves of 16 devices.

3.4. MNIST Image Encoding for Reservoir Input

To demonstrate the temporal computing potential of the OECT devices, images from the MNIST dataset (4 × 4 grayscale) were used as input stimuli. Each 2D image was unrolled into a one-dimensional vector of 16 pixels and converted into a time-series voltage waveform. Pixel intensity was linearly mapped to a gate voltage range. Each voltage level was applied as a short pulse such as 20 ms with a fixed inter-pulse interval.

This procedure transformed static spatial information into a temporally varying signal, suitable for stimulating dynamic ionic-electronic behavior in OECTs. The reservoir state was probed by monitoring IDS in response to the complete input sequence.

Specifically, pixel intensity was linearly mapped to a gate voltage range from 0.0 V to 0.6 V. Each voltage level was applied as a short pulse with a pulse width of 20 ms and a fixed inter-pulse interval of 20 ms, recorded at a sampling rate of 1 kHz.

3.5. Feature Extraction and Classification

Every single picture's current answer was recorded by an ever-changing wave over time. An example of the original MNIST digit image used as input is shown in Figure 10. From here on out we see our set with all these sliding window statistics like Local Current Peak's Area Under Curve or AUC, Derivative Signature, Recovery Time Constant. The above mentioned features constituted high dimensional state vector to be fed to the linear classifier.

A softmax regression model was trained to map extracted features to one often digit classes (0 - 9). Training using a small training set with 16 MNIST images and evaluated it on a validation set which consisted of another 500 images. And then checked for the model's performance through model accuracy as well as confusion

matrix. Backpropagation or recurrent feedback is absent, hence simplicity in the RC readout.

The feature set extracted from the temporal trajectory includes Root Mean Square (RMS) current, Peak Width, Integrated Area (AUC), and Curvature Change. These features were evaluated across 10 virtual node intervals, resulting in a total feature-vector dimension of 40 per image (4 features × 10 intervals). Prior to classification, the feature vectors underwent Z-score normalization. A softmax regression model (Adam optimizer, learning rate = 0.01, 100 epochs) was then trained to map these vectors to the ten digit classes (0 - 9).

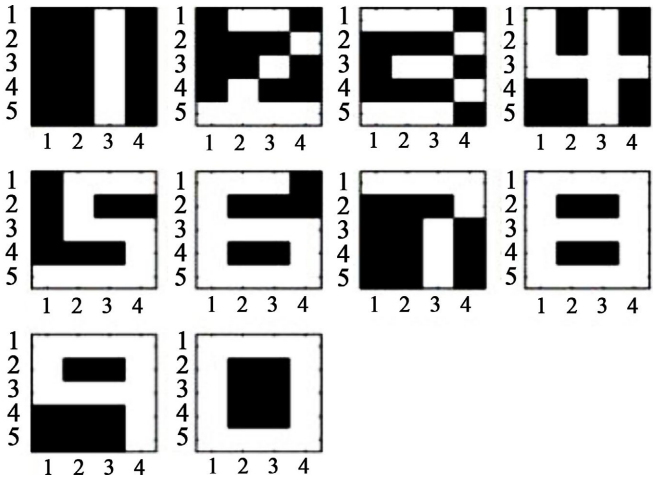

Figure 10. Original MNIST image.

4. Results Analysis

4.1. OECT Electrical Performance

The fabricated PEDOT:PSS-based OECTs displayed excellent transistor characteristics under aqueous gating. Transfer curves revealed clear switching behavior, with current decreasing as V_G became more positive. This behavior corresponds to the injection of cations into the PEDOT:PSS channel, which neutralizes holes and leads to dedoping of the material. The devices operated in depletion mode, consistent with the intrinsic characteristics of PEDOT:PSS.

Transconductance values exceeded 1.2 ms for devices with 5 μm channel lengths, indicating strong amplification capability. Output curves showed typical saturation behavior at higher VDS, confirming channel modulation. Devices exhibited low leakage and minimal hysteresis drift over multiple cycles, highlighting the reliability of the fabrication process.

4.2. Synaptic Behavior under Pulse Gating

In terms of investigating if these could work as neuromorhic function, gate pulses that mimicked a neuron spike going through. Single pulse leads to IDS decreasing for moment, then recovering gradually; similar to IPSC. Pairs of pulses when applied shortly after each other had an increased response from second pulse com-

pared to the first one, this is referred to as PPFS.

Further characterization under varying pulse intervals demonstrated dynamics analogous to spike-timing-dependent plasticity (STDP) and frequency-dependent plasticity (FDP). Specifically, the paired-pulse facilitation (PPF) was quantified by a facilitation index $\left(A_2/A_1\right)$ consistently greater than 1, confirming the device's ability to integrate temporal information. These synaptic behaviors arise from the ionic diffusion and retention dynamics within the PEDOT:PSS matrix, providing the essential short-term memory required for physical reservoir computing. While preliminary, these results suggest the OECT's potential for complex neuromorphic functions, though the present study focuses primarily on leveraging the measured STM and PPF for pattern recognition.

4.3. Response to MNIST Image Input

OECT reservoir was stimulated with temporally-encoded MNIST digit images. The OECT reservoir was stimulated with temporally-encoded 4 × 4 MNIST digit images. Each pixel's intensity was linearly mapped to a gate voltage range (0.0 V to 0.6 V), applied as a 20 ms pulse followed by a 20 ms interval, resulting in a 0.64-second total sequence per image (16 pixels × 40 ms). The resulting drain current $\left(I_{DS}\right)$ trajectories were unique to each input pattern, reflecting the complex interaction between the input sequence and the device's internal ionic states.

The nonlinear transformation of inputs via ionic-electronic interaction resulted in a rich temporal trajectory in the IDS domain. Despite using only a single OECT as the reservoir node with time multiplexing, the output carried high-dimensional features, including local nonlinearity, fading memory, and dynamic saturation.

4.4. Feature Space Construction and Classification Results

For each I_{DS} trajectory, four key features were extracted: Root Mean Square (RMS) current, Peak Width, Integrated Area (AUC), and Curvature change. These features were sampled across 10 equivalent time intervals (as shown in **Figure 11**), resulting in a 40-dimensional feature vector per image (4 features × 10 intervals). These vectors underwent Z-score normalization before being fed into a softmax regression model (Adam optimizer, learning rate = 0.01).

To evaluate the computational utility of the OECT reservoir, the achieved accuracy (78.6%) was compared with the theoretical baseline of a linear classifier (e.g., Softmax) operating directly on raw 4 × 4 pixel intensities. For such extremely low-resolution inputs, a purely linear readout without non-linear feature mapping typically yields an accuracy between 40% and 50% [12]. The significant performance margin achieved in this work quantitatively demonstrates that the OECT's intrinsic ionic-electronic dynamics effectively project the low-dimensional spatial inputs into a high-dimensional, linearly separable feature space, which is the hallmark of effective physical reservoir computing.

Representative output waveforms corresponding to different MNIST digits are shown in **Figure 12**. The classification errors primarily involved ambiguous digits,

and confusion matrices showed that most digits were correctly clustered. The results validate the ability of a single dynamic OECT node to act as a physical reservoir capable of spatial and temporal signal transformation.

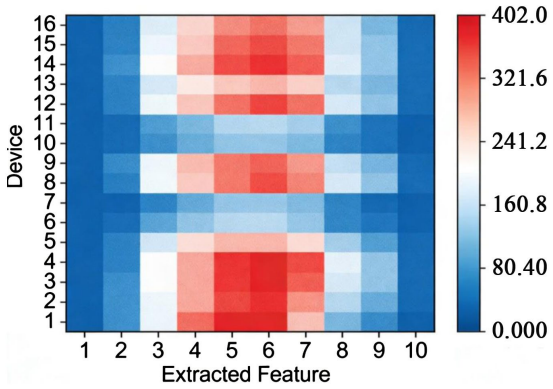

Figure 11. Extracted value at 10 equivalent time intervals from 16 channels after pulse application.

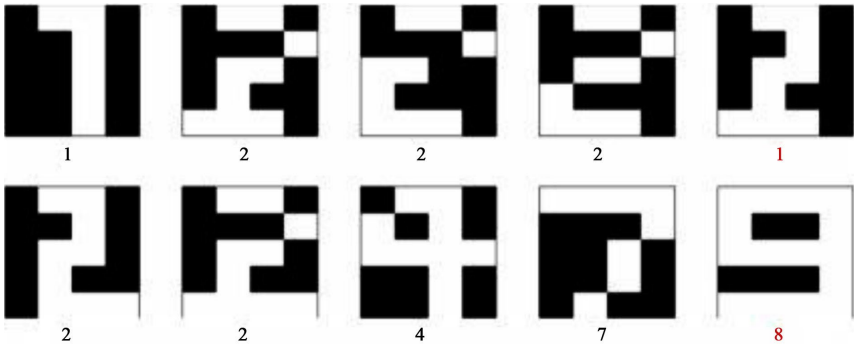

Figure 12. MNIST image output.

The classification success is rooted in the device's temporal integration capacity. As detailed in the methodology (Section 2.5), the delay-memory task confirmed an average memory capacity of 7 - 9 pulses (~140 - 180 ms), which aligns with the pulse intervals used in the MNIST task.

5. Discussion

The PEDOT:PSSOECT can be dynamic nodes in physical reservoir computing which is applied to the temporal vision tasks in this research. Their unique electrochemical action that supports synaptic flexibility, temporal coding, and nonlinear adjustment of input sequence. And importantly these can also be made totally flexible; the devices are fully flexible and compatible with low-cost, solution-processable fabrication.

Future work will explore scaling the reservoir by using many parallel OECT's, improving ion mobility and retention, and adding in CMOS-compatible readout circuits. More alternatives including n-type OECT channels or ionic gels might extend bandwidth and Stability. Finally, these kinds of systems can lead to bio-

mimetic classifiers, adaptive edge processor and full soft Neuromorphic machine.

So it has to do a little bit of explaining here, but what's up is that they've got an output of high-performance and flexible physical reservoir computer systems (PRC), these being on the basis of organic electrochemical transistors (OECT). Using multilayer photolithography, made very small and stable on bendable polyimide, was done with very fine OECT arrays. The PEDOT:PSS-based OECTs have abundant intrinsic synaptic behaviors such as short term memory (STM), paired pulse facilitation (PPF) and frequency dependent plasticity, which are basically determined by the coupled ionic-electronic transport and volumetric doping mechanisms.

6. Conclusion

In summary, this work demonstrates a flexible physical reservoir computing system based on OECTs. By leveraging the coupled ionic-electronic transport of PEDOT:PSS, we successfully transformed spatial MNIST data into temporal sequences for high-accuracy recognition (78.6%). Our results show that a single-node OECT, through time-division multiplexing, can provide sufficient non-linear dynamics and memory for complex pattern recognition. This architecture offers a promising path for low-power, biocompatible neuromorphic hardware in wearable edge-computing applications.

Conflicts of Interest

The authors declare no conflicts of interest regarding the publication of this paper.

References

[1] Wulf, W.A. and McKee, S.A. (1995) Hitting the Memory Wall: Implications of the Obvious. *ACM SIGARCH Computer Architecture News*, **23**, 20-24.

[2] Mead, C. (1990) Neuromorphic Electronic Systems. *Proceedings of the IEEE*, **78**, 1629-1636. https://doi.org/10.1109/5.58356

[3] Jaeger, H. (2001) The "Echo State" Approach to Analysing and Training Recurrent Neural Networks. GMD Report 148.

[4] Tanaka, G., Yamane, T., Héroux, J.B., Nakane, R., Kanazawa, N., Takeda, S., *et al.* (2019) Recent Advances in Physical Reservoir Computing: A Review. *Neural Networks*, **115**, 100-123. https://doi.org/10.1016/j.neunet.2019.03.005

[5] van de Burgt, Y., Lubberman, E., Fuller, E.J., Keene, S.T., Faria, G.C., Agarwal, S., *et al.* (2017) A Non-Volatile Organic Electrochemical Device as a Low-Voltage Artificial Synapse for Neuromorphic Computing. *Nature Materials*, **16**, 414-418. https://doi.org/10.1038/nmat4856

[6] Rivnay, J., Inal, S., Salleo, A., Owens, R.M., Berggren, M. and Malliaras, G.G. (2018) Organic Electrochemical Transistors. *Nature Reviews Materials*, **3**, Article 17086. https://doi.org/10.1038/natrevmats.2017.86

[7] Bernards, D.A. and Malliaras, G.G. (2007) Steady-State and Transient Behavior of Organic Electrochemical Transistors. *Advanced Functional Materials*, **17**, 3538-3544. https://doi.org/10.1002/adfm.200601239

[8] Khodagholy, D., Doublet, T., Quilichini, P., Gurfinkel, M., Leleux, P., Ghestem, A., *et al.* (2013) *In Vivo* Recordings of Brain Activity Using Organic Transistors. *Nature Communications*, **4**, Article No. 1575. https://doi.org/10.1038/ncomms2573

[9] Jaeger, H. (2002) Tutorial on Training Recurrent Neural Networks, Covering BPPT, RTRL, EKF and the "Echo State Network" Approach. GMD Report 159.

[10] Lukoševičius, M. and Jaeger, H. (2009) Reservoir Computing Approaches to Recurrent Neural Network Training. *Computer Science Review*, **3**, 127-149. https://doi.org/10.1016/j.cosrev.2009.03.005

[11] Du, C., Cai, F., Zidan, M.A., Liu, H., Zhang, Q., Li, W., *et al.* (2017) Reservoir computing Using Dynamic Memristors. *Nature Communications*, **8**, Article No. 2204.

[12] Ballarini, D., Gianfrate, A., Panico, R., Opala, A., Ghosh, S., Dominici, L., *et al.* (2020) Polaritonic Neuromorphic Computing Outperforms Linear Classifiers. *Nano Letters*, **20**, 3506-3512. https://doi.org/10.1021/acs.nanolett.0c00435